Testing and modeling of constant magnetic field cylindrical magnetoelectric sensors output characteristics

Karol KUCZYNSKI[1]*, **Piotr BILSKI**[1], **Adrian BILSKI**[2], and **Jerzy SZYMANSKI**[3]

[1] Warsaw University of Technology, Faculty of Electronics and Information Technology, Institute of Radioelectronics and Multimedia Technology, Poland
[2] Warsaw University of Life Sciences, Poland
[3] Kazimierz Pulaski University of Technology and Humanities in Radom, Faculty of Transport, Electrical Engineering and Computer Science, Poland

Abstract. The paper presents the novel concept of the magnetoelectric sensor constructed using the amorphous glass ribbon. Its output characteristics (voltage pattern), conditions of work and experimental results are presented. The novel construction allows for minimizing the demagnetizing field in the core of the sensor and linearization of the characteristics between the magnetic field and obtained voltage. Conducted experiments were aimed at determining the sensor operation in the presence of the constant magnetic field (H_{DC}). The main concern of the tests was to verify the linear dependency between the H_{DC} value and the amplitude of the output voltage. Next, the computer model representing the sensor behavior in the constant magnetic field is described. The model implements the parameter identification task based on the regression algorithms. The presented work shows that the proposed device can be used to measure the weak magnetic field and the dependency between the output signal amplitudes and the constant component in the measured magnetic field is approximately linear. This enables measurements of even weak fields.

Key words: magnetoelectric effect; magnetostriction; magnetometers; amorphous magnetic materials; piezoelectric materials.

1. INTRODUCTION

Measurements of the magnetic field strength have important applications in the operation of mechanical and electronic systems. They are used in magnetic field sensors or biomedical applications. The proposed new concept is low-power energy harvesting, where the existence of the magnetic field may cause the acquisition of the electric charge as the result of the weak current flow. The important problem to solve here (leading to new sensor inventions) is the ability to detect even the weakest signal changes and obtain the linearity of the characteristics combining the magnetic field amplitude and the generated voltage in the whole range of operation. To maximize the sensor sensitivity it must operate in the resonance frequency (which is one of the design parameters).

Characteristics of the designed magnetic sensors have been analyzed in the past [1, 2]. In [1] a review of magnetoelectric sensors is presented, and in [2] the physical basics of magnetoelectric sensors is given. In [3] the voltage characteristics on the output of the sensor operating in the resonance were presented. The relation between the magnetic field and the voltage was close to linear, which is desired. On the other hand, in [4] the output characteristics of the magnetoelectric sensor were obtained based on the third harmonics analysis. Such a

construct does not ensure the positive verification of the sensor correct operation, because for the zero-field strength the sensor response is also zero.

The more complex designs of the vortex magnetic field sensor include ring or cylinder construct. In [5] the multiferroic heterostructures were put on the outside of the cylinder with the controlled thickness of each layer. In [6] the Metglas/Piezoelectric (PZT – Plumbum Zirconium Titanium) laminates with the open and closed magnetic circuit were designed in the form of a ring. Such structures have high sensitivity and are independent of the location of the center of the vortex field. The sensitivity of 5.426 V/A in the resonance frequency of 174.4 kHz is obtained.

Presented designs show much potential for using magnetoelectric sensors in various applications. However, the remaining problems include the maximization of the sensitivity and maintaining the linearity of the voltage-magnetic field strength characteristics. The following paper presents the analysis of the magnetic field sensor operation which exploits the magnetoelectric effect. First, the device work regime is presented. Next, the experiments revealing the relation between the magnetic field strength and the measured electric signals are described. The experimental setup and results of examinations are presented as well. After verifying the sensor capabilities (especially regarding linearity in the input-output characteristics), these dependencies are confirmed by the computer, regression model. The experiments show that it is possible to measure and model the linearity of the sensor characteristics.

*e-mail: karol.kuczynski@pw.edu.pl

K. Kuczynski, P. Bilski, A. Bilski, and J. Szymanski

The content of the paper is as follows. Section 2 presents the fundamentals of the magnetic field sensor operation, explaining its purpose and work regime. In Section 3, the magnetostriction effect in the designed sensor is presented. Section 4 contains the experimental setup for determining the linearity and the hysteresis loop of the sensor. In Section 5, experimental results are presented. In Section 6, the mathematical model of the sensor output of signal nonlinearity and linearity is discussed. The summary and future prospects are presented in Section 7.

2. OPERATION OF THE MAGNETIC FIELD SENSOR

The considered sensors measure the strength of the magnetic field, which is difficult because such fields are usually weak. As they have the vector form, it is essential to determine their length and direction. In most cases, sensors are designed to detect a changing field [7]. Their work regime is to measure the alternate components and extract the constant field strength from them. This also allows one to measure electrical current in the power lines. The advantage of the changing field sensors is their ability to work without an external power source. The nonlinearity of the relation between the magnetic field and the generated voltage has a negative effect on measurement accuracy. The measured voltage also depends on the type and thickness of the piezoelectric material. It is desired to have lower resonance frequencies (the kHz range), as the magnetic field generator in the sensor will be simpler.

The hybrid magneto-piezoelectric magnetic sensors exploit the magnetoelectric effect. Magnetoelectricity is the interaction between the dielectric polarization of the material and the applied magnetic field [8].

Usually, the piezoelectric element is used to generate an alternating oscillation signal responsible for strains in the amorphous ribbon that lead to the modification of the magneto crystalline anisotropy [9]. Both piezoelectric and amorphous elements are joined using the viscous fluid or glued avoiding the mechanical tensions of a rigid adhesive and allowing for the transmission of vibrations at high frequencies. The best working mode is in the resonance of the longitudinal vibrations in the piezoelectric plate, where the amplitude oscillations are large enough (in the range of single volts). Beyond this resonance frequency [10], the sensor loses the null condition (i.e., zero response to a zero external magnetic field), which allows for determining if the device is working when no field is present [9]. The direction of the constant magnetic field may be determined, though the vector length remains unknown. Such flat sensor constructions (i.e., located on the two-dimensional surface) are characterized by the open magnetic circuit. In consequence, the demagnetizing field in the core of the sensor is created. It is treated as a disturbance, which should be eliminated, because of suppressing the output signal. This problem can be solved by introducing the closed magnetic circuit into the sensor [5,6].

The use of a closed magnetic core enables measurement of the constant magnetic field (of single A/m). The approach exploits the alternating exciting field of the known frequency superimposed on the unknown constant magnetic field strength.

3. SENSOR WITH THE MAGNETOSTRICTION EFFECT IN RING-SHAPED AMORPHOUS MATERIALS

The designed sensor (initially presented in [10], where the influence of the Earth's constant field on the magnetic field strength measurement accuracy was analyzed) detects the constant magnetic field (in contrast to [11], for instance, where alternating fields are processed) using the magnetostriction effect. Its advantage over other existing approaches is the closed magnetic circuit thanks to the cylindrical shape. This allows for maximizing sensitivity thanks to reducing the demagnetizing field. It is treated as a disturbance because its direction is opposite to the measured field thus decreasing its strength.

3.1. Sensor structure

The designed sensor consists of magnetic and piezoelectric elements combined into one structure [12]. The former has the ring shape of the magnetostrictive amorphous ribbon (Magnetic Alloy 2605Co) and is placed around the piezoelectric tube as presented in Fig. 1. The x and y axes are in the plane of the tube base, while the height of the ring is located along the z axis (which is important for the resonance frequency calculations). The tube-shaped sample PZ27 produced by the Ferroperm Piezoceramics A/S was used for the tests due to the maximum relative dielectric constant at 1 kHz, giving the maximum deformation sensitivity [13]. The selected materials determine the sensor sensitivity. The magnetic components define the magnetostrictive strain, while the piezoelectric one is responsible for the strain sensitivity. The concept of the closed magnetic circuit creates new possibilities for detecting and measuring constant magnetic fields.
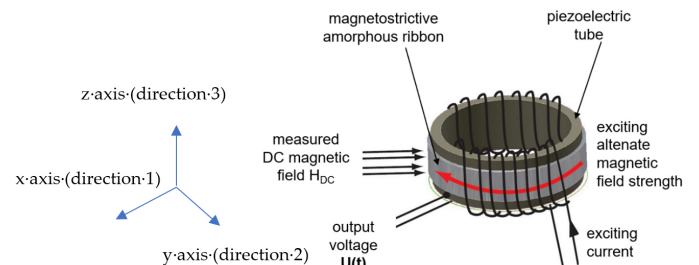

Fig. 1. Schematic diagram of the cylindrical magneto-piezoelectric magnetic field sensor [12, 15]

The physical dimensions of the sensor are as follows. The PZ27 tube has external (d_e) and internal diameters (d_i) of 24 mm and 20 mm, respectively, while its height l is 15 mm. The amorphous ribbon is 10 mm wide and 50 mm thick. The tube thickness (2 mm) was selected to obtain the maximum material transverse resonance frequency f_{rt} (where the sensor sensitivity is maximal) [14]:

$$ f_{rt} = \frac{1}{\pi \cdot (d_e - d_i)} \cdot \sqrt{\frac{1}{s_{hk} \cdot \rho_1}}, \tag{1} $$

where s_{hk} is the elasticity coefficient and ρ_1 is the material density. For PZ27 s_{hk} in the directions $h = 1$ (x axis) and

$k = 3$ (z axis) is equal to $28.6 \cdot 10^{-12}$ m^2/N, while $\rho_1 = 7.7 \cdot 10^3$ kg/m^3 [13]. To suppress the cost of the device, the off-the-shelf tube was used with the maximum thickness available (user-defined tube construction is possible, though complicated and expensive). This allowed for calculating $f_{rt} \approx 170$ kHz. The longitudinal resonance frequency is calculated as follows [14]:

$$f_{rl} = \frac{n}{2 \cdot l_h} \cdot \sqrt{\frac{1}{\rho_1 \cdot s_{hk}}}, \qquad (2)$$

where n is the harmonic number (here 1) and l_h is the sensor height (as above, equal to 15 mm). For PZ27 in the direction z (i.e. $h = 3$ and $k = 3$) $s_{hk} = 23 \cdot 10^{-12}$ m^2/N [11], which gives the first harmonic component for $f_{rl} \approx 79.2$ kHz.

The application of the amorphous ribbon, instead of the well-established Terfenol-D [6, 11], allows for obtaining a higher measurement resolution, which makes it sensitive to a weak magnetic field around the wire with the current. The piezo-electric tube deformation (as a reaction to the increase of the field strength) is nearly linear, induced around 0.1 µm/m magnetostrictive strain (in contrast to highly magnetostrictive Terfenol-D, which is around 2000 µm/m) [16]. Also, attaching the ribbon to the external layer of the ring (and not to the base as in [9]), enables the accurate measurement of the field inside the ring and makes the solution useful as the sensor. The closed magnetic circuit minimizes the demagnetizing field and the noise including from eddy currents. Similarly, the proposed solution is more accurate than the alternative design presented in [6], because while sensing the magnetic field strength around the dc cable, the measurement is done in a position equally distant from the wire. The measuring element, i.e., amorphous ribbon, is 50 mm thin, while the thicker layer will collect more disruptions and could be used for energy harvesting.

3.2. Magnetostrictive properties of the sensor

An external field (through the magnetostrictive effect [17]) produces a mechanical strain which is transferred into the piezo-electric element, causing the dielectric polarization P [18]. It is proportional to the magnetic field strength H through the second rank ME-susceptibility tensor α [18]:

$$P = \alpha H. \qquad (3)$$

In the magnetic field, the magnetostriction (depending on the magnetostrictive component – here the amorphous ribbon) generates the mechanical strains transmitted to the piezoelectric component. The strain drives the electric polarization of the component through the piezoelectric effect [19]. The magnetoelectric effect can be used for many applications like smart sensors [1–3,7,20], energy harvesters [21–25] or in signal processing operations as the data acquisition module (working as the antenna, receiving the data, further processed by the hardware-based algorithms) [7, 24].

The main factor influencing the magnetoelectric properties of composites is their magnetostriction λ. It depends on changes in the physical dimensions of the soft magnetic materials induced by the applied external magnetic field. Magnetostric-

tion is characterized by the relative change in the sensor body size [26]:

$$\lambda = \Delta l / l, \qquad (4)$$

where l is the initial length of the magnetic material and Δl is its change imposed by the external magnetic field.

Typically, the field drives changes in the physical dimensions of magnetic materials while maintaining their volume. This causes a positive change in one dimension while the other one is negative, depending on the particular material. For this reason, the longitudinal magnetostriction factor $\lambda_| = (\Delta l / l)_|$ is determined, characterizing the relative change in the length of the magnetic material along the applied external magnetic field. The transverse magnetostriction coefficient $\lambda_\perp = (\Delta l / l)_\perp$ denotes the change in the length of the magnetic sample perpendicular to the applied magnetic field. These parameters are used to define the anisotropic magnetostriction λ_τ [27, 28]:

$$\lambda_\tau = \lambda_| - \lambda_\perp \qquad (5)$$

and the volume magnetostriction λ_υ:

$$\lambda_\upsilon = \lambda_| + 2\lambda_\perp. \qquad (6)$$

If the starting demagnetized state is isotropic, the results obtained at magnetostrictive saturation are: $\lambda_| = -2$ and $\lambda_\perp = \lambda_s$. This defines the saturation magnetostriction constant λ_s of the isotropic material. For this reason, the volume magnetostriction variation is indeed zero (longitudinal changes are cancelled by the perpendicular ones) [29, 30].

It is assumed that λ can be approximated using the quadratic function at low magnetic field strength H (i.e. $\lambda_\tau \approx \alpha \cdot H^2$) and the saturation magnetostriction λ_s is present in the strong field (i.e., $H \gg H_s$). Then the magnetostriction can be described as follows [4]:

$$\lambda(H) = \lambda_s \cdot \left(1 - e^{\alpha \cdot H^2}\right), \qquad (7)$$

where α is the constant coefficient, measured in the units of the magnetic field strength, i.e. [Oe^{-2}] or [(A/m)$^{-2}$]. The output voltage from the magnetoelectric sensor as a function of the constant magnetic field H_{DC} can be expressed as follows [4]:

$$\begin{aligned} U(H_{DC}) &= U_0 + U_1 \cos(2\pi ft) + U_2 \cos(4\pi ft) \\ &\quad + U_3 \cos(6\pi ft) + \cdots, \end{aligned} \qquad (8)$$

where $U_0 = A \cdot d_{31} \left[\lambda(H_{DC}) + \lambda_s(\alpha - 2\alpha^2 H_{DC}^2) \cdot h^2\right]$ is the constant voltage component, $U_1 = 2Ad_{31}\lambda_s \alpha h \cdot H_{DC}$ is the amplitude of the first harmonic component, $U_2 = Ad_{31}\lambda_s(\alpha - 2\alpha^2 H_{DC}^2) \cdot h^2$ is the amplitude of the second harmonic component, $U_3 = 0.5Ad_{31}\lambda_s \alpha^2 h^3 H_{DC}$ is the amplitude of the third harmonic component with h being the excitation magnetic field, and so on.

The presented relations were used to generate the simulated characteristics of magnetostrictive strain in the function of the magnetic field strength and the voltage obtained on the output of the sensor (Fig. 2). The characteristics were obtained

Bull. Pol. Acad. Sci. Tech. Sci., vol. 71, no. 1, p. e144583, 2023

3

K. Kuczynski, P. Bilski, A. Bilski, and J. Szymanski

through the MATLAB simulation, and then verified experimentally (see Section 5). To create the model, characteristics of materials used to build the sensor from Fig. 2 were applied: $\lambda_s = 20$ ppm, $H_{DC} = 1$ Oe (where $1 \text{Oe} = 10^3/4\pi$ A/m), $\alpha = 1 \text{ Oe}^{-2}$, $h = 3$ Oe, $f = 1$ kHz, $A = 10$, $d_{31} = 5.8 \text{ E}^{-9}$ Wb/N. Low output voltage in the simulation of the magnetoelectric sensor (Fig. 3) is the consequence of disregarding the actual shape and the structure of the sensor. In the presented case the simplified, flat (two-dimensional) model was considered, while in the actual sensor the depth will also influence the generated waveforms.
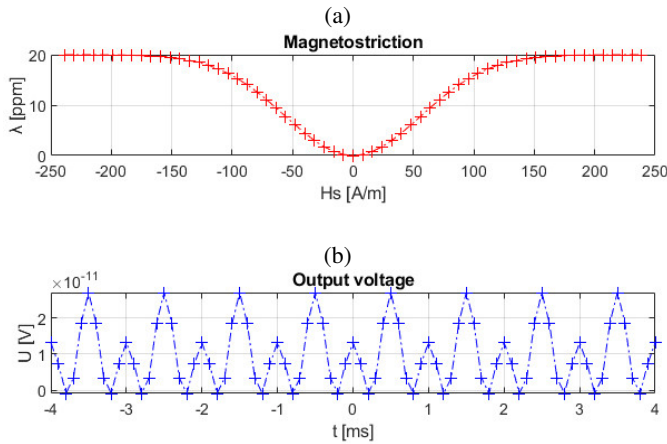
Fig. 2. The MATLAB simulation based on equation (7): magnetostriction (a), output voltage (b) from the sensor model (8)
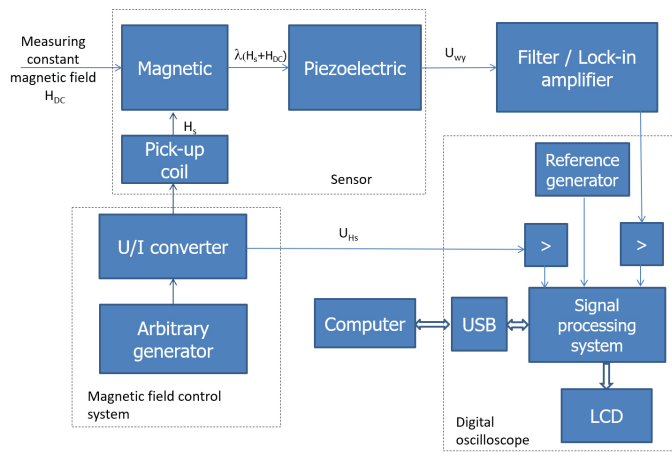
Fig. 3. Schematic block diagram of the measuring system

4. EXPERIMENTAL SETUP

To verify the characteristics of the sensor and confirm its linearity, the experimental stand was prepared. It was aimed at determining the responses of the sensor to the known magnetic field provided to its input with the weak constant field component in the background. This way it would be possible to determine the relations between specific excitations and responses.

The measurement system for measuring the sensor output voltage is shown in Fig. 3. The system consists of the pick-

up coil producing an exciting magnetic field of the analyzed device, a hybrid magneto-piezoelectric sensor and the digital measurement system. The exciting field is driven by the current generator working at 1 kHz (which is the standard frequency for testing material properties of the sensor, such as relative dielectric constant and dielectric dissipation factor [13]). The output signal from the sensor is a function of the measured constant magnetic field H_{DC}. It is processed by the measurement system containing the digital oscilloscope connected to the PC. The system allows for the visualization of the magnetoelectric field sensor characteristics.

The measurement setup allowed for determining the sensor limitations, valid throughout experiments. The Limit of Detection (LoD), defining the sensitivity of the sensor was established in the order of single A/m. This makes the device susceptible to small field values (by comparison, the Earth's field has a magnitude of around 3 to 5 A/m). The magnetoelectric coefficient α_{ME} [31] shows a relation between the magnetostriction and the constant magnetic field strength. Small values (between 0.03 and 0.08 mV/A/m) were measured.

The oscilloscope measurements (Fig. 4) allow one to obtain the voltage proportional to the excitation magnetic field H_s induced in the pick-up coil (blue pattern) according to (9) and voltage on the output of the sensor U_{pp} (purple pattern). These facilitate evaluating U_{pp} in the function of the measured constant magnetic field H_{DC} with an additional value of H_s as a parameter (see Section 5).

$$H_s = U_m \cdot \sin(\omega t). \tag{9}$$

Fig. 4. Visualization of the input and output signals in regard to the system #16 simulation

The principle of the sensor operation is in Fig. 5. To evaluate its performance, the hysteresis loops were measured. They were acquired using the oscilloscope. First, magnetic hysteresis was acquired. The alternating magnetic field H was generated on the ring-shaped core by the current flowing through the magnetizing (excitation) coil. Then the electromotive force U induced in the measurement coil was measured. It is proportional to the dynamics of changes in the magnetic stream present in the core.

The magnetostrictive hysteresis was measured by the semiconductor strain gauge in the Wheatstone half-bridge cir-
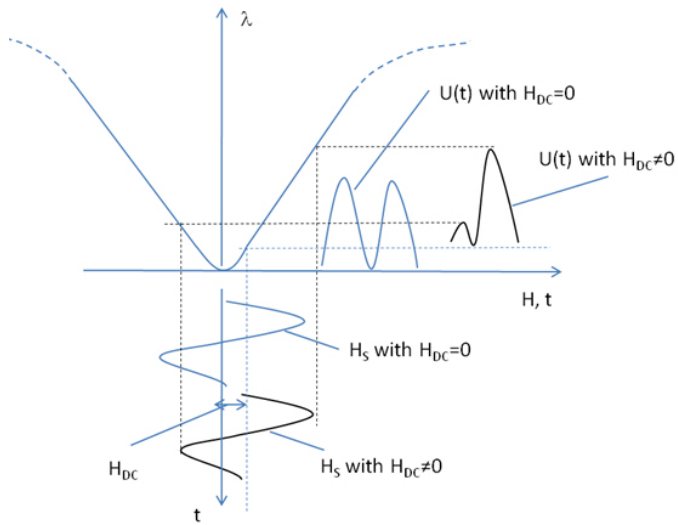
Fig. 5. Principle of the magnetoelectric sensor [4, 31]

cuit [16]. It aims to determine changes in the measured resistance ΔR based on the voltage in the imbalanced branch of the circuit.

5. EXPERIMENTAL RESULTS

The quasistatic magnetic hysteresis (i.e., obtained for 1 Hz) for the metal glass ribbon 2605 Co [32], used to construct the proposed sensor, is presented in Fig. 6. It demonstrates the behavior of the sensor (response of the material) in the changing field. The hysteresis loop implies that the material is ferromagnetic. The geometric field surrounded by the hysteresis loop determines the amount of energy required to remagnetize the material (i.e., change the direction of the magnetic domain). The magnetic induction B values are relatively large here, though the geometric (coercion) field is narrow (as is for soft materials). This implies that the energy losses during the demagnetization are small. The saturation of the hysteresis curve determines the maximum range of magnetic field changes visible for the sensor material [33].
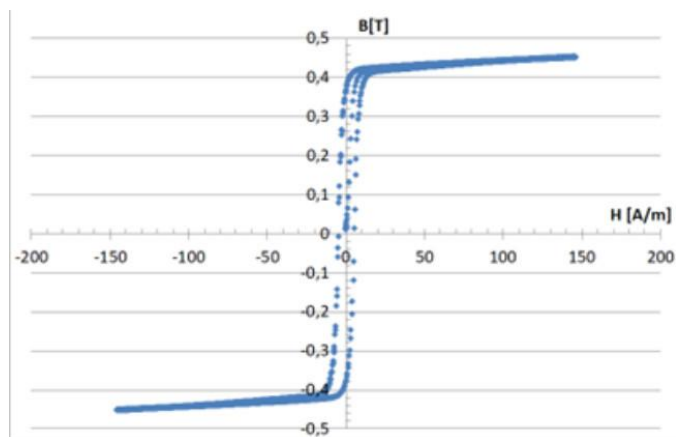

Fig. 6. Quasistatic (around 1 Hz) magnetic hysteresis loop for the metal glass ribbon 2605Co

The hysteresis loop for the 1 Hz field changes after adding the amorphous ribbon to the piezoelectric tube. This results in the strong attenuation of the loop. Figure 7 shows the deformed magnetic loop of the amorphous ribbon. Attaching it to the surface of the piezoelectric caused the attenuation of the magnetic hysteresis. Similarly to Fig. 6, the magnetostrictive loop is narrow. Both loops have identical values of the coercion field (i.e., the intersection of the magnetic hysteresis with the horizontal axis).
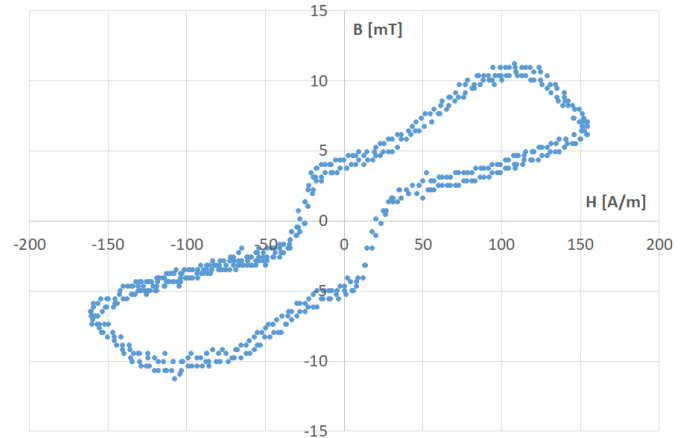

Fig. 7. Magnetic hysteresis loop for the amorphous ribbon 2605Co in the field frequency of 1 kHz

Figure 8 shows the magnetostrictive hysteresis loop. Measurements aimed to determine the strain of the magnetic material caused by the alternate and constant magnetic fields. The sensor operation is driven by the alternate field created in the coil wound up on the sensor, powered by the 1 kHz current. The device is supposed to detect the constant field, but harmonic components appear. They are the result of the time evolution of the strain induced in the magnetic layer [4]. The strain should be maximal and linearly proportional to the constant field. The first harmonic component is dominant, while others can be neglected.
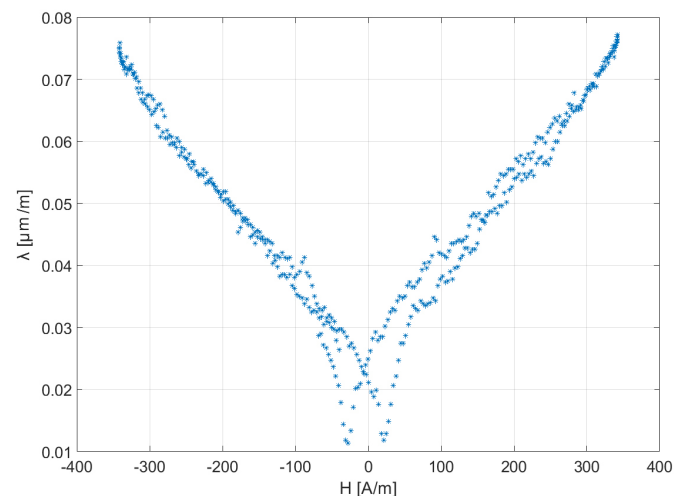

Fig. 8. Magnetostrictive hysteresis loop for the amorphous 2605Co ribbon attached to the piezoelectric material PZ27

The shape of the measured hysteresis loop is similar to that obtained from simulations (see Fig. 2a). Differences are mainly due to the limited accuracy of the simulation, especially in approximating the hysteresis loop with the exponential function. Magnetostriction values are different because the two-dimensional model was used to represent the three-dimensional ring.

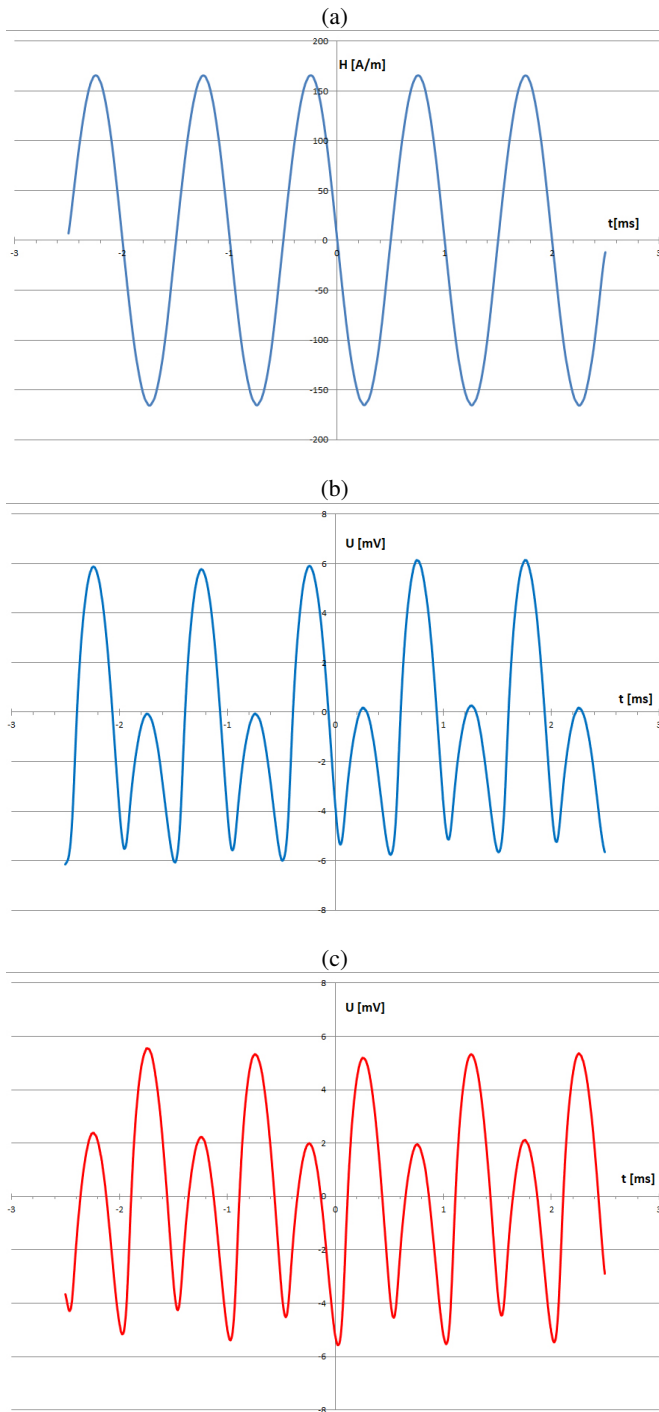Similarly, Fig. 9 shows the behavior of the sensor in the alternating magnetic field, as was simulated in Fig. 2b. The wave-

form of the exciting magnetic field H_s is shown in Fig. 9a. The sensor output signal with the measured constant magnetic field $H_{DC} = 50$ A/m is shown in Fig. 9b. The output signal of the sensor measured in the presence of the constant magnetic field $H_{DC} = -50$ A/m, (but in the opposite direction), is shown in Fig. 9c.

6. MODELING AND MEASUREMENT OF THE CHARACTERISTICS OF THE OUTPUT SENSOR

The measured characteristics indicate the ability of the device to detect the magnetic field. The most important aspects are the ability to detect the weak field and the measurement accuracy, which also depends on the linearities of the characteristics. Although the hysteresis curves (Figs. 6–8) are important in determining the sensor work regime, the practical aspect of its operation requires determining the relation between the magnetic field strength and the measured voltage. The linearity of the sensor is its desired trait, as it determines the ability to assess the actual value of H_{DC} based on the voltage measurement. This section covers the sensor analysis of the output characteristics, including the measurements and modeling.

6.1. Measurement of output characteristics

The measurement system from Fig. 4 allows one to perform measurements regarding the relation between U_{pp} and H_{DC}. The former may be extracted either from the overall measured voltage or its first harmonic component. Figure 10 shows that the actual relation between H_{DC} and the 1st harmonic peak-to-peak voltage is linear. Unfortunately, this solution is not practical, as isolating the harmonic component from the measured voltage requires using complex and expensive equipment. Therefore, it cannot be used in the actual sensor.
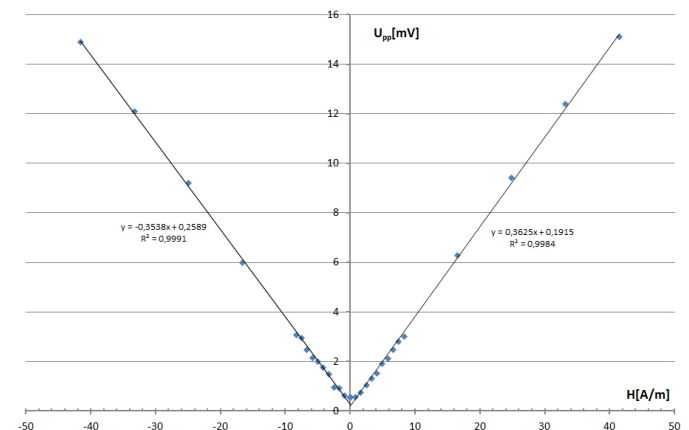
Fig. 9. The operation of the sensor: (a) exciting magnetic field H_s, (b) sensor output signal for $H_{DC} = 50$ A/m, (c) sensor output signal for $H_{DC} = -50$ A/m

Fig. 10. Characteristics of the 1-st harmonic peak to peak output voltage of the sensor as a function of the H_{DC} with constant value of exciting magnetic field $H_s = 82$ A/m, and straight lines approximating the characteristics

The practical usage of the device (measurement applications, energy harvesting, etc.) requires determining the relation between the actual value of H_{DC} and the corresponding measured U_{pp}. This way the measured quantity would be, for instance,

6

Bull. Pol. Acad. Sci. Tech. Sci., vol. 71, no. 1, p. e144583, 2023

presented in digital form and make the device usable as a smart sensor.

Figure 11 presents the spectrum of the magnetic field-induced voltage. It shows the input of the subsequent harmonic components to the acquired signal. The fundamental component (at 1 kHz) dominates here. It is proportional to the magnetic field and influences the shape of the current waveform most intensely.
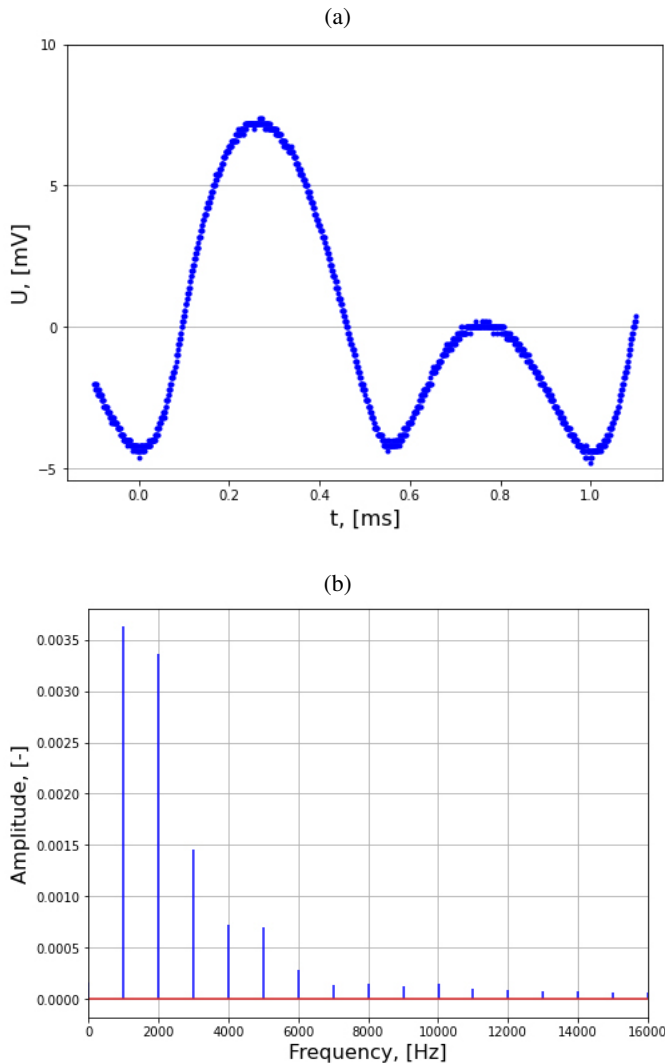
(a)

(b)

Fig. 11. Voltage waveform in the sensor output (a) and its amplitude spectrum (b)

Practical applications of the sensor require determining the value of H_{DC} based on the overall voltage, including all harmonic components. It is measured in a presence of the exciting magnetic field H_s of the known strength. As shown in Fig. 12, this characteristic is nonlinear in the whole range of the measured field. This creates a problem for the practical sensor application, especially regarding the accurate indications based on the induced current or voltage signals. Although solving it through sensor construction may be difficult (see [30]), the easier solution is heuristic modelling of the curve, as shown in Section 6.2.
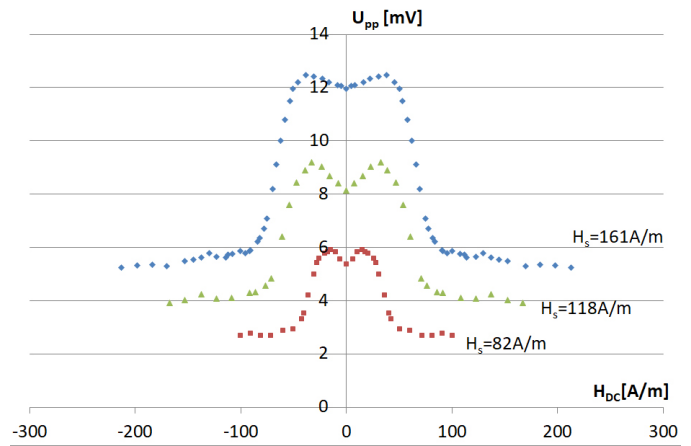

Fig. 12. Characteristics of the output voltage U_{pp} of the sensor as a function of H_{DC} with constant value of exciting magnetic field H_s

6.2. Modeling of the output characteristics

Both types of characteristics, i.e., presented in Figs. 10 and 12, were modeled using methods presented in Appendix A.1. Due to the simplicity of characteristics in Fig. 10, the linear regression method was used (introduced in detail in Appendix A.1 and A.2). Coefficients of the functions, i.e., (12) and (13) generated on the available measurement points are presented in Table 1.

Table 1
Values of the linear approximation coefficients (a and b) and R^2 of Fig. 14 depending on the excitation field H_s

H_{DC} range	a	b	R^2
positive	2.0111	$-5E^{-15}$	0.9394
negative	2.9411	$-1E^{-14}$	0.9424

The proposed modeling method is straightforward but requires a complex and expensive measurement system. Characteristics from Fig. 12 require a more sophisticated mathematical apparatus but can be performed in the typical measurement procedure (without the additional equipment). Due to the widespread popularity and high regression accuracy, Multilayered Perceptron (MLP) was used (its configuration is presented in Appendix A.3).

The MLP results are presented in Figs. 13–15, while the values of $\overline{MSE}$ (14) for optimal MLP configurations are in Table 2 and Table 3 (for LOOCV and RRSSCV, respectively – see Appendix A.3, where n_{h1} and n_{h2} represent the number of neurons in the first and the second hidden layer). For $H_s = 82$ [A/m] and 118 [A/m] the accuracy allows for a close representation of the actual characteristics, though by using the more complex ANN. For 161 [A/m] the problem is the range (−50; 50) [A/m], where the characteristics are too flat. This is despite applying rather large networks to the task. Although the optimal structures (minimizing $\overline{MSE}$) is complex and may be affected by overfitting, obtaining better results may be difficult due to two factors. First, modeling a single input (besides the bias, which
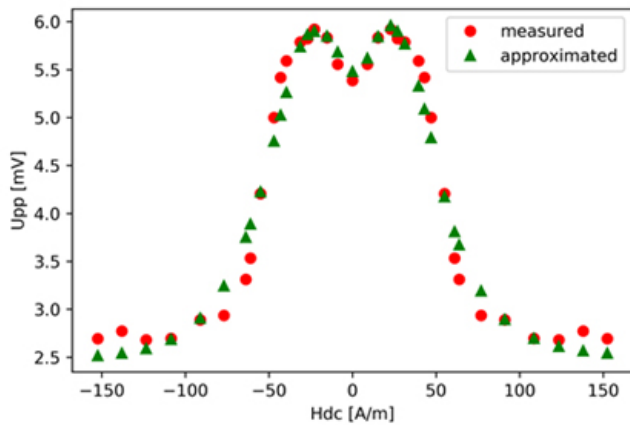
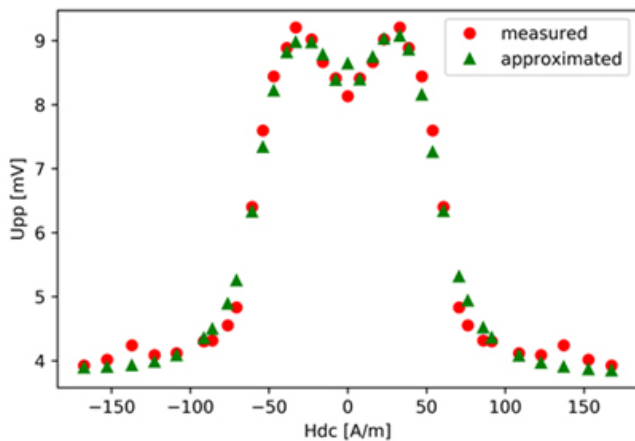**Fig. 13.** Modeling of U_{pp} characteristics for $H_s = 82$ [A/m]

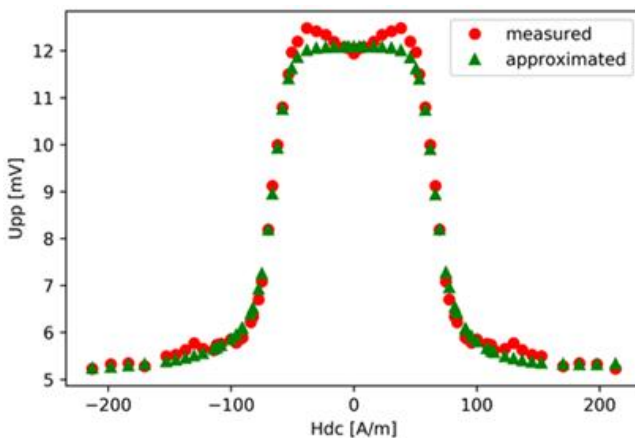**Fig. 14.** Modeling of the U_{pp} characteristics for $H_s = 118$ [A/m]

Fig. 15. Modeling of the U_{pp} characteristics for $H_s = 161$ [A/m]

remains constant, only its weights change) into the single output requires the second hidden layer. The first one obtains only one variable to weigh and adds it to the second weighted constant. The second problem is the small number of training examples, which stipulates more sophisticated structures for regression.

Table 2
Optimal MLP configurations with the corresponding MSE values for LOOCV

H_s [A/m]	n_{h1}	n_{h2}	MSE
82	6	52	0.0393
118	61	9	0.0740
161	12	54	0.0469

Table 3
Optimal MLP configurations with the corresponding MSE values for RRSSCV (7:3 ratio)

H_s [A/m]	n_{h1}	n_{h2}	MSE
82	5	26	0.2024
118	7	47	0.2733
161	11	62	0.1422

In reality, simpler networks can be used, as many configurations have similarly low $\overline{MSE}$. A comparison of various ANN configurations (to change the number of neurons in the first hidden layer) is shown in Fig. 16. Although the optimal MSE values are around 0.1, similar results (between 0.14 and 0.16) can be achieved for smaller networks. The compromise between these two factors must be made during the practical implementation of the model.
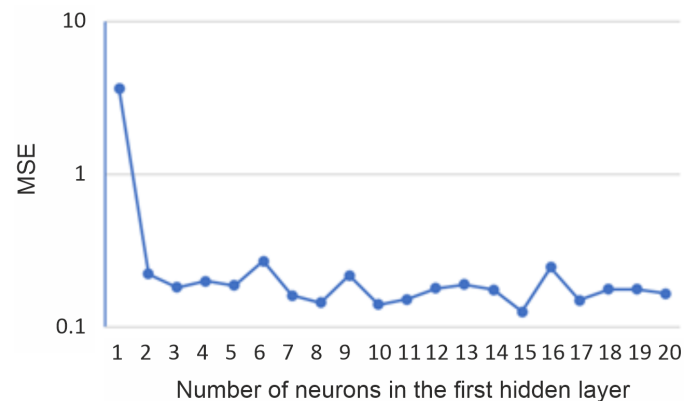

Fig. 16. MLP MSE for increasing number of neurons in the first layer, with $n_{h2} = 5$ ($H_s = 82$ [A/m])

Modeling the output characteristics is crucial in the case of linearity enhancement. If the actual value of H_s is given, for which the ANN was trained, the mirror reflection of the modeled characteristics may be superimposed on the measured one, giving the nearly linear curve. This, however, requires adding the processing module to the sensor, which will be able to process the measured voltage, linearize it and present the estimated constant magnetic field in the digital form (similarly to [34]). Experiments with the sensor extension are the next step of our research.

8

Bull. Pol. Acad. Sci. Tech. Sci., vol. 71, no. 1, p. e144583, 2023

A comparison between cross-validation (see Appendix A.3) approaches shows that indeed the number of samples for training MLP is too small, as MSE significantly increases if just their fraction is eliminated from L (i.e., the learning data set; see Appendix A.3). Also, the complexity of networks increases with the value of H_s (which can be explained by the higher range of modeled values and the flatter central part of the characteristics). The experiments were limited to changing the configuration of two hidden layers.

For each curve (depending on the value of H_s), the optimal ANN structure is different, which calls for a single, uniform model of the sensor characteristics. Unfortunately, based only on the H_s and H_{DC} inputs, it is not possible to create a single ANN architecture applicable to represent all measurement configurations, unless the number of material parameters, for which measurements are taken, will be significantly increased (which requires multiple additional laboratory experiments). Simulations performed for the single MLP with the aggregated data from all sensors allowed only for the rough approximation of the actual characteristics (with $\overline{MSE}$) above 0.5, which is not acceptable). Therefore, currently, to properly model the particular characteristics, the separate network must be selected, based on the given value of H_s.

7. CONCLUSIONS

The development of the magnetoelectric magnetic field sensor with the closed circuit creates new possibilities for measuring low constant magnetic field H_{DC}. This sensor is characterized by the closed magnetic circuit, which minimizes the demagnetizing field in the core of the sensor. The device can be used as a practical tool to test the constant magnetic field which is comparable to the magnetic field of the Earth. This enables us to find the direction of the DC magnetic field which was not possible in the magnetoelectric field sensors with open circuits. The cylindrical magnetoelectric sensor creates new possibilities for producing highly magnetostrictive materials.

Modeling of the measured characteristics shows that it is possible to provide a relatively simple computing structure allowing us to describe the relation between H_{DC} and U_{pp}. For practical reasons, the heuristic model should be as simple as possible, which requires a compromise between the model accuracy and its complexity. It can also be used to enforce the linearization of the sensor characteristics by adding an ANN model as the additional component of the device.

Future research requires implementing other modeling algorithms, especially with respect to their applicability in an embedded system that would be part of the smart sensor. In addition, an analysis of the computational requirements for the actual embedded system should be performed.

A. APPENDIX: MODELING DETAILS

A.1. Modeling prerequisites

The modeling procedures were implemented to fit the measurement data in both cases presented. The aim was to provide a function that combined the values of H_{DC} and U_{pp}. In both cases, the regression task must be solved, i.e., finding the function that best fits the measurement data points in a computationally reasonable way. The obtained results would lead to a design of the smart sensor providing information about the measured magnetic field in the digital form, i.e., the binary codeword.

Modeling of sensors and their characteristics is usually performed through analytical methods, where multiple differential equations must be constructed. An example is the modeling of the Wiegand sensor, where the Simulink scheme was applied [35]. As these are complex and do not consider all phenomena, simplified approaches are searched for. For example, hysteresis is often modeled using the Preisah operator [36]. The relatively new approach is to use a heuristic approach, such as the artificial neural network (ANN) [37]. The autoencoder is the deep learning network applicable to represent the sensor behavior in industrial process control [38].

To create such models, data sets are required. In the case of the first harmonic component, three sets were created, according to the performed laboratory experiments, as Fig. 12 shows. Each set has the form of a table with two parameters: H_{DC} and U_{pp}, the former being the input to the model, and the latter the produced value of the evaluated parameter.

The standard tool for evaluation of the modeling accuracy is the mean square error (MSE), which allows one to determine the distances between the computed and measured voltages:

$$MSE = \frac{1}{N} \cdot \sum_{i=1}^{N} \left(U_{pp}[i] - U_m[i] \right)^2. \tag{10}$$

Here, U_{pp} is the measured voltage value for the specific magnetic field strength, U_m is the modeled value, and N is the number of considered data points. Alternatively, the R^2 measure may be used.

Furthermore, the linear regression for the 1st harmonics of U_{pp} can be evaluated with the R^2 measure, where a is the coefficient of the $U_{pp} = a \cdot H_{DC} + b$ modeling function (created to represent the measurement points in Fig. 11).

$$R^2 = \frac{\left(\overline{H_{DC} \cdot U_{pp}} - \overline{H_{DC}} \cdot \overline{U_{pp}} \right)^2}{\left(\overline{H_{DC}^2} \right) \cdot \left(\overline{H_{DC}}^2 \right)} = a^2 \cdot \frac{\overline{H_{DC}^2} - \overline{H_{DC}}^2}{\overline{U_{pp}^2} - \overline{U_{pp}}^2}, \tag{11}$$

where $\overline{H_{DC}}$ and $\overline{U_{pp}}$ are average values of the measured constant magnetic field and the peak-to-peak voltage, respectively.

A.2. Linear regression modeling

The value of U_{pp} extracted from the 1st harmonic component may be modeled by the straight lines, depending on the range of the actual values of H_{DC}. The main problem is that the measured quantity must be divided into two parts, each modeled separately by the straight line, generally represented as $U_{pp} = a \cdot H_{DC} + b$, based on the set of measured points. The coefficients a (12) and b (13) are adjusted to minimize the used measures (10) and (11) [39, 40]. This way, the best approxima-

Bull. Pol. Acad. Sci. Tech. Sci., vol. 71, no. 1, p. e144583, 2023

9

K. Kuczynski, P. Bilski, A. Bilski, and J. Szymanski

tion of the measured field characteristics is found.

$$a = \frac{\overline{U_{pp} \cdot H_{DC}} - \overline{U_{pp}} \cdot \overline{H_{DC}}}{\overline{U_{pp}^2} - \overline{H_{DC}^2}}$$

$$= \frac{\sum_{i=1}^{N} \left(H_{DC}[i] - \overline{H_{DC}} \right) \cdot \left(U_{pp}[i] - \overline{U_{pp}} \right)}{\sum_{i=1}^{N} \left(H_{DC}[i] - \overline{H_{DC}} \right)^2}, \tag{12}$$

$$b = \overline{U_{pp}} - a \cdot \overline{H_{DC}} = \frac{\overline{U_{pp}} \cdot \overline{H_{DC}^2} - \overline{H_{DC}} \cdot \overline{H_{DC} \cdot U_{pp}}}{\overline{H_{DC}^2} - \overline{H_{DC}}^2}. \tag{13}$$

A.3. Heuristic modeling of the output characteristics

The advantage of the heuristic regression method is the automated extraction of input-output relations. Among multiple approaches (such as support vector machines [41], kriging or M5 model Tree [42]), the MLP was selected. This type of ANN is well established in industrial applications and widely used for tasks where the modeled data are not affected by the extensive amount of noise (as experiments in the presented case show). The network consists of at least one hidden layer with computational units and a single output neuron with the linear activation function. Applications of MLP for the parametric identification of technical systems are known [43, 44]. In the presented research the task was to model characteristics from Fig. 13 with the maximum accuracy.

The application of the MLP (with the structure like in Fig. 17) for the task consisted in training the network on the available data sets for the preselected structure, i.e., the number of layers and the number of neurons in each layer. Training is performed using the error backpropagation method, implemented in the Python language (sci-kit framework). Its quality is determined using the *MSE* (10), although the R^2 measure (11) may also be used. The MLP optimization process consisted of repeated training-evaluation schemes performed for the increased complexity of the ANN (i.e., after adding neurons). The network with the minimum *MSE* and the simplest structure is selected.
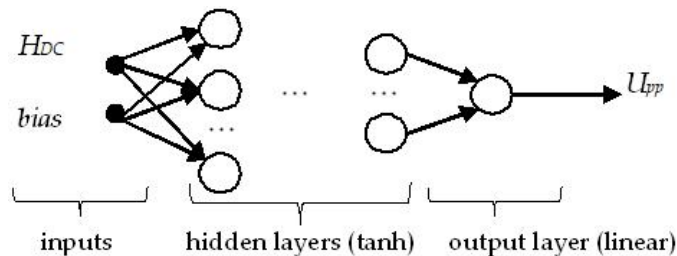

Fig. 17. Structure of the MLP applied to model the output characteristics of the sensor

Another problem to consider during the ANN regression application is its evaluation, disregarding the actual training set. Usually, cross-validation (CV) is used, where the training samples (forming the set L) are randomly selected from the original

dataset D, while all others form the validating set T. Repeating this scheme *K* times allows one to obtain more generalized (averaged) information about the performance of the particular ANN structure (where MSE_k is the ANN error in the *k*-th trial):

$$\overline{MSE} = \frac{1}{K} \cdot \sum_{k=1}^{K} MSE_k. \tag{14}$$

Usually, repeated random sub-sampling CV (RRSSCV) is used, where the sizes of the ratio between the training and testing sets (respectively, |L| and |T|) are parameterized (for example, as 7:3 or 8:2). Due to the small number of samples taken from the experiments (that is, 35 for $H_s = 82$ and 118 and 67 for $H_s = 161$), leave one out CV (LOOCV) was also used. This is the exhaustive method where the number of iterations is equal to the size of the data set and the validating set is always a single sample (though different in every iteration). RRSSCV was applied with $|L| = 0.7 \cdot |D|$ and $|T| = 0.3 \cdot |D|$.

REFERENCES

[1] M. Bichurin *et al.*, "Magnetoelectric magnetic field sensors: A review," *Sensors*, vol. 21, p. 6232, 2021, doi: 10.3390/s21 186232.

[2] J. Das *et al.*, "Control of magnetic and electric responses with electric and magnetic fields in magnetoelectric heterostructures," *Appl. Phys. Lett.*, vol. 96, p. 222508, 2010, doi: 10.1063/1.3443715.

[3] J.L. Prieto, C. Aroca, E. Lopez, M.C. Sanchez, and P. Sanchez, "Reducing hysteresis in Magnetostrictive-Piezoelectric Magnetic Sensors," *IEEE Trans. Magn.*, vol. 34, pp. 3913–3915, 1998, doi: 10.1109/20.728303.

[4] D.A. Burdin, D.V. Chashin, N.A. Ekonomov, Y.K. Fetisov, and A.A. Stashkevich, "High-sensitivity dc field magnetometer using nonlinear resonance magnetoelectric effect," *J. Magn. Magn. Mater.*, vol. 405, pp. 244–248, 2016, doi: 10.1016/j.jmmm.2015.12.079.

[5] D. Xie, Y. Wang, and J. Cheng, "Length dependence of the resonant magnetoelectric effect in Ni/Pb(Zr,Ti)O3/Ni long cylindrical composites," *J. Alloy. Compd.*, vol. 615, pp. 298–301, 2014, doi: 10.1016/j.jallcom.2014.06.208.

[6] D.T.H. Giang *et al.*, "Magnetoelectric Vortex Magnetic Field Sensors Based on the Metglas/PZT Laminates," *Sensors*, vol. 20, p. 2810, 2020, doi: 10.3390/s20102810.

[7] H. Palneedi, V. Annapureddy, S. Priya, and J. Ryu, "Status and perspectives of multiferroic magnetoelectric composite materials and applications," *Actuators*, vol. 5, p. 9, 2016, doi: 10.3390/act5010009.

[8] D. Filippov, V. Petrov, V. Laletsin, N. Poddubnaya, and G. Srinivasan, "Giant Magnetoelectric Effect in Composite Materials in the Region of Electromechanical Resonance," *Tech. Phys. Lett.*, vol. 30, pp. 6–8, 2004, doi: 10.1134/1.1646700.

10

Bull. Pol. Acad. Sci. Tech. Sci., vol. 71, no. 1, p. e144583, 2023

[9] N.H. Duc and D.T. Huong Giang, "Magnetic sensors based on piezoelectric–magnetostrictive composites," *J. Alloy. Compd.*, vol. 449, pp. 214–218, 2008, doi: 10.1016/j.jallcom.2006.01.121.

[10] K. Kuczynski, A. Bilski, P. Bilski, and J. Szymanski, "Analysis of the Magnetoelectric Sensor Usability for the Energy Harvesting," *Int. J. Electron. Telecommun.*, vol. 66, no. 4, pp. 787–792, 2020, doi: 10.24425/ijet.2020.135193.

[11] S. Dong, J.-F. Li, and D. Viehland, "Vortex magnetic field sensor based on ring-type magnetoelectric laminate," *Appl. Phys. Lett.*, vol. 85, pp. 2307–2309, 2004, doi: 10.1063/1.1791732.

[12] K. Kuczynski, "Magnetic field sensor," utility model PL 067861, 2014, (in Polish), [Online] Available: https://worldwide.espacenet.com/patent/search/family/051754078/publication/PL121952U1?q=ap%3DPL121952* [Accessed: 10. Jun. 2022].

[13] Catalog Ferroperm Piezoceramics A/S. [Online] Available: bioafm.physics.leidenuniv.nl/dokuwiki/lib/exe/fetch.php?media=biospmlab:tech:ferroperm-catalogue.pdf.

[14] J. Matauschek, *Einführung in Die Ultraschalltechnik*, Berlin: VEB Verlag Technik, 1957.

[15] K. Kuczynski, "Possibilities of the application of hybrid magneto-piezoelectric junction as the magnetic field sensor," *Przegląd Elektrotechniczny*, vol. 86, no. 4, pp. 69–71, 2010 (in Polish).

[16] L. Chen, Y. Wang, T. Luo, Y. Zou, and Z. Wan, "The Study of Magnetoimpedance Effect for Magnetoelectric Laminate Composites with Different Magnetostrictive Layers," *Materials*, vol. 14, p. 6397, 2021, doi: 10.3390/ma14216397.

[17] K. Kuczynski, L. Sabut, A. Bienkowski, and G. Dymny, "Newly Developed Systems for Magnetostrictive Materials Strain Measurements," *Acta Phys. Pol. A*, vol. 113, pp. 71–74, 2008, doi: 10.12693/APhysPolA.113.71.

[18] M.D. Mermelstein and A. Dandridge, "Low-frequency magnetic field detection with a magnetostrictive amorphous metal ribbon," *Appl. Phys. Lett.*, vol. 51, pp. 545–547, 1987, doi: 10.1063/1.98394.

[19] D.A. Filippov, M.I. Bichurin, C.W. Nan, and J.M. Liu, "Magnetoelectric effect in hybrid magnetostrictive-piezoelectric composites in the electromechanical resonance region," *J. Appl. Phys.*, vol. 97, p. 113910, 2005, doi: 10.1063/1.1929865.

[20] C.M. Leung, J. Li, D. Viehland, and X. Zhuang, "A review of applications of magnetoelectric composites: from heterostructural uncooled magnetic sensors to energy harvesters to highly efficient power converters," *J. Phys. D, Appl. Phys.*, vol. 51, p. 263002, 2018, doi: 10.1088/1361-6463/aac60b.

[21] B. Pozo, J.I. Garate, J.Á. Araujo, and S. Ferreiro, "Energy harvesting technologies and equivalent electronic structural models – review," *Electronics*, vol. 8, p. 486, 2019, doi: 10.3390/electronics8050486.

[22] F. Narita, M. and A. Fox, "Review on piezoelectric, magnetostrictive, and magnetoelectric materials and device technologies for energy harvesting applications," *Adv. Eng. Mater.*, vol. 20, p. 1700743, 2018, doi: 10.1002/adem.201700743.

[23] S. Priya and D.J. Inman, Eds. *Energy harvesting technologies*, Springer Science+Business Media, LLC, 2009.

[24] J. Kaleta, *Smart magnetic materials. Structure, manufacturing, testing properties, application*, Wroclaw University of Technology Publishing House, Wroclaw, 2013 (in Polish).

[25] K. Kuczynski and G. Parzonko, "Possibilities of the energy recovery from the environment (energy harvesting) and other ways of powering electric vehicles," *elektro.info*, vol. 179, no. 11, pp. 58–61, 2019 (in Polish).

[26] M.J. Dapino, "On magnetostrictive materials and their use in adaptive structures," *Struct. Eng. Mech.*, vol. 17, no. 3-4, pp. 303–329, 2004, doi: 10.12989/sem.2004.17.3.

[27] P. Guzdek, W. Grzesiak, P. Zachariasz, and G. Kolaszczynski, "Magnetostrictive properties of multiferroic composites", *Przegląd Elektrotechniczny*, vol. 92, pp. 29–32, 2016, doi: 10.15199/48.2016.09.07 (in Polish).

[28] Y. Uwatoko, I. Umehara, M. Ohashi, T. Nakano, and G. Oomi, "Chapter 252 Thermal and Electronic Properties of Rare Earth Compounds at High Pressure", *Handbook on the Physics and Chemistry of Rare Earths*, Elsevier, 2012, doi: 10.1016/B978-0-444-54316-5.00001-6.

[29] É. du Trémolet de Lacheisserie, D. Gignoux, and M. Schlenker, *Magnetism – Fundamentals, Materials and Applications*, Springer, New York, 2002, doi: 10.1007/978-0-387-23062-7.

[30] D. Jiles, *Introduction to Magnetism and Magnetic Materials*, 3rd ed., CRC Press, 2015, doi: 10.1201/b18948.

[31] G. Srinivasan, S. Priya, and N.X. Sun, *Composite Magnetoelectrics – Materials, Structures, and Applications*, Woodhead Publishing Series in Electronic and Optical Materials: Number 62, Elsevier, 2015.

[32] Catalog Metglas 2605Co. [Online] Available: https://metglas.com/brochures/

[33] P. Dadhich, R. Prajesh, R. Mukhiya, and S.S. Kumar, "Sensitivity and Linearity Enhancement of Piezoresistive Pressure Sensor Using Stress Concentration Structure," *IEEE 16th India Council International Conference (INDICON)*, India, 2019, doi: 10.1109/INDICON47234.2019.9029015.

[34] C. Chun-Chi, C. Chao-Lieh, and L. Yi, "All-digital linearity enhancement technique for time-domain smart temperature sensors," *Procedia Eng.*, vol. 87, pp. 1247–1250, 2014, doi: 10.1016/j.proeng.2014.11.409.

[35] X. Sun, T. Yamada, and Y. Takemura, "Output characteristics and circuit modeling of the wiegand sensor," *Sensors*, vol. 19, p. 2991, 2019, doi: 10.3390/s19132991.

[36] P. Frydrych, R. Szewczyk, and J. Salach, "Magnetic fluxgate sensor characteristics modeling using extended preisach model," *Acta Phys. Pol. A.*, vol. 126, pp. 18–19, 2014, doi: 10.12693/aphyspola.126.18.

[37] W. Zhu *et al.*, "Predicting and optimizing coupling effect in magnetoelectric multi-phase composites based on machine learning algorithm," *Compos. Struct.*, vol. 271, p. 114175, 2021, doi: 10.1016/j.compstruct.2021.114175.

[38] Y. Wang and X. Yan, "Soft sensor modeling method by maximizing output-related variable characteristics based on a stacked autoencoder and maximal information coefficients," *Int. J. Comput. Intell. Syst.*, vol. 12, no. 2, pp. 1062–1074, 2019, doi: 10.2991/ijcis.d.190826.001.

[39] J. Fox, *Applied regression analysis and generalized linear models*. Third Edition, Sage Publications, Inc., 2016.

[40] T. Hastie, R. Tibshirani, and J. Friedman, *The elements of statistical learning: data mining, inference, and prediction*. 2nd Ed., Springer New York, 2017, [Online]. Available: https://link.springer.com/content/pdf/10.1007/978-0-387-84858-7.pdf?pdf=button%20sticky [accessed: 10. Jun. 2022].

[41] K. Behrooz, M. Cihan, and K. Ozgur, "Comparison of four heuristic regression techniques in solar radiation modeling: kriging method vs rsm, mars and m5 model tree," *Renew. Sust. Energ. Rev.*, vol. 81, pp. 330–341, 2018, doi: 10.1016/j.rser.2017.07.054.

[42] M. Rohani, H. Jazayeri-Rad, and M. Behbahani, "Continuous prediction of the gas dew point temperature for the prevention the foaming phenomenon in acid gas removal units using artificial intelligence models," *Int. J. Comput. Intell. Syst.*, vol. 10, pp. 165–175, 2017, doi: 10.2991/ijcis.2017.10.1.12.

[43] J.A. Lopez and E. Caicedo, "Parametric identification using multilayer perceptron," *International Conference on Industrial Electronics and Control Applications*, 2005, p. 4, doi: 10.1109/icieca.2005.1644375.

[44] I. Rojek, D. Mikołajewski, J. Nowak, Z. Szczepański, and M. Macko, "Computational intelligence in development of 3d printing and reverse engineering," *Bull. Pol. Acad. Sci. Tech. Sci.*, vol. 70, no. 1, p. e140016, 2022, doi: 10.24425/bpasts.2021.140016.